DEGRADATION OF SUPERCONCUCTING RF CAVITY PERFORMANCES BY EXTRINSIC PROPERTIES

J. Halbritter, FZK, IMF I
Postfach 3640, 76021 Karlsruhe, Germany

Abstract

The intrinsic surface resistance of superconductors $R_{BCS}(T,f,B)$ is degraded by extrinsic effects which actually limit applications, e.g., by rf breakdown or severe heat load. Examples for extrinsic effects are, rf residual losses R_{res} increasing with rf electric field E_p or rf magnetic field B_p or heating ΔT of the cavity surface relative to the He-bath. With the now available material qualities and surface preparations, gross local defects are rare and global degradations show up. Aside of the rf residual losses R_{res} related to the Nb-Nb_2O_5 interface, extrinsic field dependencies are encountered reaching from Q-slope, i.e. $\delta R \propto R_{BCS}(T,f)\,(1 + \gamma(B_{rf}/B_c)^2 + \eta (B_{rf}/B_c)^4 +)$ with $\gamma > \eta$ as the begin of a Taylor series and $B_c(0) \simeq 0.2$ T, to Q-drop, i.e. $\delta R^E \propto \exp(-c/E_p)$ without field emission, and for Nb films or heavily corroded Nb, to $R_{hys} \propto \omega\, B_{rf}/j_{cJ}$ with j_{cJ} the critical current density of weak links. For carefully prepared and oxidized Nb $R_{res}(T,f) \gtrsim 2\ (f/GHz)^2 n\Omega$ have been attained. In bulk Nb cavities immersed in He a Q-slope with $\gamma\ (T < 2.17K = T_\lambda) \lesssim 0.2 - 3$ has been reached turning above T_λ to $\gamma \gtrsim 10 - 20$ confirming ΔT heating by the Kapitza thermal boundary resistance as main cause. Thermal interface resistances in sputtered Nb cavities yield, e.g. $\gamma(T) \simeq 20 - 90$, simulating an exponential R(B)-increase via the exponential $R_{BCS}(T + \Delta T,f,B)$ increase. The Q-drop is explained by interfacial tunnel exchange with Nb_2O_5. Internal surfaces, i.e., weak links, as they occur by oxidation along grain boundaries or at other defects, e.g., in cold worked Nb, yield hysteresis losses R_{hys} at rather low fields. Because of $j_{cJ}(T \lesssim T_c/2) \simeq$ const, $R_{res}(T \leq T_c/2)$ and $R_{hys}(T \leq T_c/2)$ are T-independent for Nb, like the interface losses $\delta R \propto \exp(-c/E_p)$, whereas the Q-slope replicates via $\gamma(T)R_{BCS}(T)$ the BCS surface resistance in its T-dependence for $R_{BCS}(T + \Delta T) > R_{res} + R_{hys} + R^E$. All observations, up to date, can be explained in this frame work, showing the importance of detailed analysis of R(T,f,B)-dependencies and pointing toward locally piled up rf losses transferred to interfaces and then to He being the key for further improvements of peak fields and for the reduction of rf losses.

INTRODUCTION

The now available excellent Nb qualities free of gross defects, with resistance ratios RRR ≥ 100, with surface treatments reaching from buffered chemical polishing (BCP), to electropolishing (EP) followed by high pressure (≥ 80bar) water rinsing (HPR) [1] has yielded rf breakdown fields above $B_{C1}(T \geq 1.6\ K) \leq 0.17$ T, corresponding to surface peak fields $E_p > 70$MV/m [2]. Those excellent results have been reached despite global deteriorations related, e.g., to oxidation or heat resistances discussed in Sects. 2 and 3.

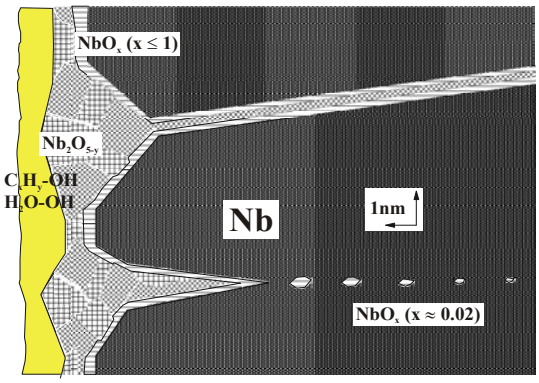

Fig. 1: Nb surface with crack corrosion by oxidation by Nb_2O_5 volume expansion (factor 3). Nb_2O_{5-y}-NbO_x weak links/segregates (y, x < 1) extend up to depths between 0.01 – 10 µm for good – bad Nb quality and weak - strong oxidation [4b]. For sputtered Nb the oxidation proceeds preferably along already existing island boundaries due to growth. Embedded in the adsorbate layer of H_2O/C_xH_yOH (≥ 2 nm) being chemisorbed by hydrogen bonds to $NbO_x(OH)_y$, adsorbate covered dust is found. This dust yields dynamically enhanced field emission (EFE [5b]).

The consequences of oxidation sketched in Fig. 1 are summarized in Sect. 2 material science wise, whereas in Sect. 3 the surface resistances R(T,ω,B) due to intrinsic and extrinsic effects are discussed as function of temperature T, frequency ω and B_{rf} fields. These discussions focus on newly clarified aspects, like enforced oxidation along grain boundaries or dislocations and on different Nb_2O_{5-y} qualities, mentioned shortly in [3].

The amount and size of NbO_x cluster depend on nucleation and treatment, as discussed in Section 2, especially sizes will grow by segregation with 90 - 150 °C baking. Those NbO_x cluster with their depressed order parameter Δ^* yield localized states easily driven out of the thermal equilibrium causing the peak at $B_{max} \simeq$ 1-2mT in $R_{BCS}(T,\omega,B)$ and rf induced superconductivily stabilizing those regions, as discussed in Sect. 3 – 5.

The different Nb_2O_{5-y} qualities and thicknesses cause exponentially increasing electric interface losses $R^E \propto \exp(-c/E)$ being nonalytical, in contrast to surface resistance increases by heating with $\delta R^H \propto \gamma^* B^2$ in lowest order in B.

Bulk Nb with wall thickness d ≈ 2mm submersed in LHe show a jump in $\gamma^*(T)$ at $T_\lambda \simeq 2.17$ K by about a factor 5 – 10 proving the dominance of ΔT heating by the Kapitza resistance R_K over the diffusive Nb thermal conductivity. Sputtered Nb shows enhanced $\gamma \gtrsim 20$ values depending on treatment. All γ enhancements are likely caused by locally enhanced losses R_{res} being transferred with negligible diffusive broadening to interfaces by ballistic phonons or quasiparticles, discussed in Section 3 – 5.

With this basis, extrinsic and intrinsic low and high rf field surface resistances are analyzed in Sect. 4 and consequences and ways to improve the rf cavities will be discussed.

CHEMISTRY AND MORPHOLOGY OF THE Nb-Nb_2O_5-ADSORBATE SYSTEM

In Fig. 1, a typical Nb surface is shown being homogenized and cleaned by heating in UHV or in a Ti-enclosure above 1000 – 1400°C followed by BCP or EP [1,2] removing about 40 - 100μm of the Nb surface containing defects by, e.g., machining nucleating enforced oxidation [3,4]. Starting from the vacuum side, by its strong hydrogen bonds the NbOOH surface is coated by 20 – 100 monolayers (ML) of H_2O and hydrocarbons [5,6], where the last 2 ML cannot be removed by UHV annealing below about 400°C. Embedded in this soup, dust coated by water and hydrocarbons may cause surface flashover and enhanced field or secondary electron emission [5]. Dust is reduced drastically by intense HPR making so surface field strengths above 10MV/m possible [1,4a]. By the high energy per bond of 7 eV in the metallic interface oxide NbO_x($x \approx 1$) and of 5eV in the dielectric Nb_2O_5, any Nb surface gets oxidized instantaneously at pressures above 10^{-10} Torr below about 10^3 K to thicknesses up to 1 – 3 nm Nb_2O_5 by the Cabrera-Mott process [4b]. There O^{--} is driven by the potential through the Nb_2O_{5-y} oxidizing the metallic NbO_x to Nb_2O_5 by a factor above three volume expansion, therewith the Nb is strained yielding cracks and NbO_x cluster injection into Nb. Hence the Nb and its surface layers, e.g., Nb_2O_5 are compressed shifting all clumsy ions (PO^{+}_2,…) out of O-octahedra network making up the surface as known from the compact part of the double layer at metal-electrolyte interfaces. Nb_2O_{5-y} is nanocrystalline by its rigid, edge connected NbO-octahedra blocks with $\phi = E_c - E_F \simeq 1$eV as difference of Fermi energy E_F and conduction band E_c which in turn get side connected via crystallographic shear planes (CS) with $\phi \simeq 0.1$ eV, where oxygen vacancies occur easily yielding for 300 K surface oxides with $n_L \lesssim 10^{19\text{-}20}/cm^3$ localized states at E_F [4c]. The tunnel transport through Nb_2O_{5-y} barriers follow CS channels showing up most clearly for barrier width $d \geq 1.5$ nm via resonant tunneling [4c], being normal conducting for $z_L \gtrsim 0.3$ nm. The states $n_L(z \leq 2\text{nm})$ are in fast ($< 10^{-10}$ sec) interface tunnel exchange (ITE) with Nb conduction electrons of density n_m as sketched in Fig. 2. For the conduction electrons ITE yield surface scattering described by a surface mean free path l_s and normal conducting n_L (z_L) yield rf residual losses R_{res} and tunnel leakage currents. The actual exchange with Nb_2O_{5-y}-states under influence of an rf electric field $E^{\perp}(t)$ correspond to dielectric interface losses R^E [7].

The unperturbed bulk Nb has a $T_c = 9.25$ K and an average energy gap $\Delta_o(0) = 1.56$ meV, where 2 At % O degrades T_c down to 7 K and Δ_o down by 20 to 30% [4]. The 2 – 3 ML thick metallic NbO_x ($x \approx 1$) – layer between Nb_2O_{5-y} and Nb has a reduced energy gap $\Delta^* < \Delta_o$. Inside the Nb below 600 K Nb_2O_{5-y}-weak links or NbO_x ($0.2 \geq x \geq 0.02$) precipitate (Fig. 1) out of the Nb-O lattice gas [4a]. By the enhanced volume of NbO_x-precipitates and of Nb_2O_{5-y}-interfaces the surrounding Nb lattice is compressed enhancing $\Delta^* > \Delta_o$ by up to 10% whereas at NbO_x itself $\Delta^* < \Delta_o$ is depressed by 10 to 20% [4]. The intermingled enhanced and depressed Δ^* regions of size below about 5nm << ξ_F smear the BCS density of state and depress the average energy gap to $\Delta < \Delta_o$. For defective Nb, e.g. RRR $\lesssim$ 50 or by coldworking, the Nb_2O_5

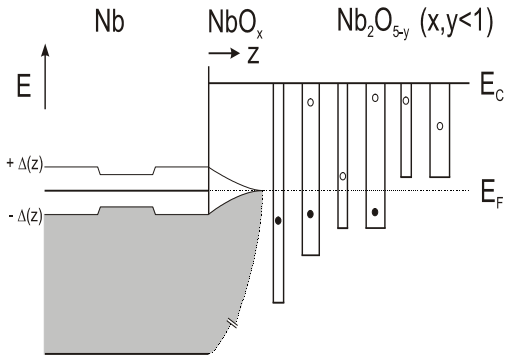

Fig. 2: Band structure at Nb-NbO_x-Nb_2O_{5-y} interfaces with E_c-$E_F \approx$ 0.1 – 1 eV as barrier heights for tunneling along crystallographic shear planes (~ 0.1 eV) or of Nb_2O_{5-y} crystallites (~ 1 eV). Added is the superconducting energy gap $\Delta^*(z)$ being reduced in NbO_x clusters or interfaces. By their volume expansion those clusters locally enhance T_c^* and $\Delta^* > \Delta_o$ in adjacent Nb by the uniaxal strain yielding a smeared BCS DOS.

filled weak links extend between $w \simeq 0.2$ - 1μm deep into Nb [3], in contrast to RRR > 100 well annealed Nb with $w < 0.1$ μm sketched in Fig. 1.

Like the Nb-O-system below 600K, hydrogen precipitates to Nb-H below about 130 K preferably to form weak links ($w \gtrsim$ 1μm) nucleating close to the surface because of the NbH volume expansion [8]. NbH_x-precipitates are removed to larger depth by lattice compression by NbO_x precipitates in the surface layer. Better is UHV annealing above 800°C, where H_2 is evaporated, and then sealing-off the surface by Nb_2O_{5-y} to prevent H-pick-up.

INTERACTION OF RF-FIELDS WITH Nb CAVITY SURFACES

The rf fields at metallic surfaces can be separated in rotational free component rot E ≡ 0, namely $E^{\perp}$ giving rise to an electric field surface impedance $Z^E = R^E$-$i\omega\mu_o\lambda^E$ and in a divergence free component div E ≡ 0, namely $H^{\parallel}$ giving rise to rf shielding currents and magnetic surface impedance $Z^H = R^H + i\omega\lambda^H$. Whereas the dielectric surface impedance Z^E of clean metals is negligible because of $\lambda^E \leq 0.1$ nm [7], Nb-Nb_2O_{5-y} by ITE cause a measurable Z^E being discussed in Sect. 3.1. By a penetration depth λ^H ($T < T_c/2$, $f < 100$ GHz) ≥ 40nm and λ^H ($T > T_c$) > μm/$\sqrt{}$ f/GHz the shielding current cause the dominant impedance Z^H in superconducting and normal conducting rf cavities.

Electric Surface Impedance Z^E

Whereas the intrinsic Z^E of metals is negligible small [7], the localized states n_L of Nb_2O_{5-y}, at the Fermi energy E_F (Fig. 2) enhance by interface tunnel exchange (ITE) with the high DOS of Nb n_m (E_F) Z^E by several orders of magnitude. Quantitatively, the exchange is governed by a tunnel rate (Fig. 2)

$$1/\tau\,(z_L,\varepsilon) = 1/\tau\,(0,\varepsilon)\,\exp(-2\kappa z_L) \qquad (1.1)$$

with $\hbar\kappa = \sqrt{2m(E_c - E_F)} = \sqrt{2m\phi}$

with $n_m \propto 1/\tau\,(0,\varepsilon)$. This exchange defines a distance $z^*(\omega)$ up to which the localized states are in equilibrium

with the DOS of the metal for a frequency $\omega\tau(z^*) = 1 = \omega\tau(0) \exp 2z^* (\omega)\kappa$.
According to [7] Z^E is proportional to $z^*(\omega)\, n_L(z^*)$, i.e. linearly increasing with n_m, n_L and $z^*(\omega)$, i.e. exponentially with lowered barrier height ϕ. The latter is quite small along crystallographic shear planes with $\phi \approx 0.1$ eV which house the localized states $n_L \approx 10^{19\text{-}20}/cm^3$ [4]. For normal conducting Nb estimates gave with $\varepsilon = \varepsilon_r\varepsilon_o$ and $\varepsilon_r(Nb_2O_{5-y}) \approx 10 - 20$ at the interface [7] with $z^* \approx 1 - 3$ nm < d the Nb_2O_5 thickness

$$R^E (Nb - Nb_2O_{5-y}) \approx 10^{-4}\ \Omega/\varepsilon^2_r \approx 10^{-5} - 10^{-7}\ \Omega \qquad (1.2)$$

at about 1 GHz. In the superconducting state an energy gap $|\varepsilon| < \Delta$ in $n_m(\varepsilon)$ opens blocking ITE. With $2\kappa\Delta\varepsilon_r/e\beta^* = c$ for fields higher than $E^\circ_{rf} = \varepsilon_r\Delta/e\beta^* \min\{z_E^*(\omega), d\}$ ITE sets in where $ez_E\, \beta^* E^\perp_{rf}/\varepsilon_r$ overcomes the energy gap Δ. The static, geometric field enhancement factor $\beta^* < 10$ is smaller than the dynamic field enhancement factor $\beta \approx 10^2 - 10^3$ [5b]. Then R^E writes:

$$R^E = \omega\mu_o d^* e^{-c/E},\ E^\perp > E^\circ_{rf} \qquad (1.3)$$

i.e. only states between z_E and $z^*(\omega)$ cause ITE rf losses approaching for $E^\perp_{rf} \simeq 10^9$ V/m Eq. (1.2) with $d^* \propto n_m\, n_L$. Hence R^E shows an onset at E°_{rf} increasing exponentially like $\exp(-c/E_{rf})$ with $E^\perp$.
The small exponent c in Eq. (1.3) is fitted by $E^{\perp n}$ starting with $4 \le n \le 16$ with n increasing by surface smoothness and reduced n_L, i.e. not by a Taylor series [4a]. ITE in Eq. (1.3) develops out of standard field emission [7] by substituting $\phi = E_c - E_F \approx$ eV and $\beta \ge 10^2$ by $\Delta \approx$ meV and $\beta^* << \beta$ yielding as ratio between FE- and ITE-exponents $\phi/\Delta \approx 10^3$.

Intrinsic Magnetic Surface Impedance Z^H

The BCS-theory [9] is an excellent tool to obtain averaged material parameters over a $2\lambda = 80$ nm Nb surface layer as shown in [4a,b] with agreement experiment/theory above 6 orders in magnitude in R(T). The lengths describing Z^H of Nb are: the London penetration depth λ_L, the dimension of Cooper pairs ξ_F and the electron mean free path l. l is reduced to $\lambda_L/\sin 30^\circ \approx 3\lambda_L$ by inelastic surface scattering via ITE [7] by trajectories with $\theta \approx 30^\circ$ relative to the surface enhancing with $1/1 = 1/1_o + 1/1_s$

$$\lambda(T,1) \approx \lambda_L(T)\, f(\gamma)\ \sqrt{1 + \xi_F/1} \text{ with } \gamma = \lambda_L / \xi_F \qquad (2.1)$$

with $\lambda(0)\, f(\gamma) = 38$ nm by non-local effects [9]. $\lambda(T) > \lambda_L(T)$ is only weakly depending on temperature below $T_c/2$, whereas above 5K strong and preparation dependent $\lambda(T)$ increases have been reported [4b]. Especially the $\lambda(T^*_c)$ jump [3] being related to stretches of $NbO_{0.02}$-clusters with $T^*_c \approx$ 6-7 K are worth mentioning [3] being indicated in Fig. 1, extending as weak links up to $\simeq 10\mu$m deep into cold worked Nb.
In contrast to $\lambda(T)$, the surface resistance R (T,f,B) has been studied intensively in the last year because of its direct relevance to superconducting rf accelerator performance [4a]. Whereas $\lambda(T,l)$ of Eq. (2.1) are approximated very well by a superconducting momentum transport carrier density, the surface resistance needs a complex computer code [9] for the matrix elements depending sensitively on the BCS density of states close to the Fermi energy $\varepsilon = E - E_F$

$$N(\varepsilon) = N_F(0) \cdot \varepsilon / \sqrt{\varepsilon^2 - \Delta^2} \qquad (2.2)$$

and on momenta of in – and outgoing quaisparticles. Due to the BCS singularity R is enhanced yielding [9]

$$R_{BCS}(T,\omega) \approx c\omega^2\, N(\Delta)\, (\Delta + \hbar)$$
$$[f(\Delta) - f(\Delta + \hbar\omega)]M^2 \approx c^*\, \omega^2\, \Delta/kT\ \sqrt{2\hbar\omega\Delta}$$
$$\exp(-\Delta/kT);\ (T \le T_c/2,\ \hbar\omega << \Delta) \qquad (2.3)$$

Small NbO_x($x < 0.1$) clusters of sizes below 5 nm < ξ_F show a depressed order parameter $\Delta^* < \Delta_o$ compensated in part by proximity to bulk Nb, whereas their strain onto the surrounding enhances $\Delta^* > \Delta_o$. Those NbO_x-cluster smear the BCS square root singularity by $\delta\Delta^*$ yielding a reduction of the mean R_{BCS} in Eqs. (2.3) by a factor 2 at 1.5 GHz

$$R^*_{BCS}(T,f) \propto (\hbar\omega)^2 \exp(-\Delta/kT) / \sqrt{\Delta_o \delta\Delta^*}\ kT < R_{BCS}$$
$$(T,f < 10GHz) \qquad (2.4)$$

Clearly, those cluster reduce also the mean free path l, which is already reduced to $l_s \approx 3\lambda_L$ by inelastic surface scattering at n_L-sites of Nb_2O_{5-y} of Fig. 2.
At NbO_x/Nb_2O_{5-y} interface layers the energy transferred to quaisparticles is effectively transferred to phonons via localized states n_L. This is different to NbO_x-cluster depicted in Fig. 1, where quasiparticles are weakly localized by $\Delta^* < \Delta$ yielding enhanced losses by $\Delta^* < \Delta$ with an electron-phonon coupling like in bulk Nb at his temperature. This electron phonon coupling is weak as shown by the inelastic scattering time for $\hbar\omega \ll \Delta$ excitations

$$\tau_{in} \approx 1.15 \cdot 10^{-10} (T_c / T)^3 \text{ sec} \qquad (2.5)$$

which has to be compared to the quasi particle absorption rate τ_{qp} [4a]

$$\frac{1}{\tau_{qp}} = \frac{B^2_{rf}}{\hbar 2 \cdot \mu_o}\ \frac{1}{n_c \hbar\omega} \cdot \frac{R}{X} \qquad (2.6)$$

where for Nb with $n_m = 6.3 \cdot 10^{22}$/eVcm³ as density of states, $\hbar\omega \approx 10^{-5}$ eV, $B_{rf} \approx$ 1mT and $X/R \approx 200$ $\tau_{ab} \approx 10^{-8}$ sec is obtained comparable to τ_{in}. For $B_{rf} \gtrsim$ 1mT this bottleneck enhances the local electronic temperature $T^* > T$ at NbO_x-clusters and NbO_x surface layers and, thus, according to Eq. (2.3) by $\exp(-\Delta^*/kT^*)$, the absorption growth first with B. In contrast, adjacent Nb with the mean energy gap Δ, with the absorption given by $\exp(-\Delta/kT)$, the absorbed quanta easily dissipate somewhere in the Nb-wall because of $\tau_{in}\nu_F \approx 2$ nm. But in $\Delta^* < \Delta$-regions confined states overheat by $1/\tau_{qp} > 1/\tau_{in}$ holding locally. The overheating of $\Delta^* < \Delta$ regions in a second step for $B > B_{max}$ yields rf losses decrease with $T^* \to \infty$, where according to [4a]

$$R^* B^2_{rf} \approx const; B > B_{max} \qquad (2.7)$$

holds for energy independent τ_{in}. Above about $10B_{max}$ $R_{BCS} \propto \exp(-\Delta/kT)$ holds where thermal equilibrium is guarantied because of $\nu_F\tau_{in} \gg \lambda$ for quasiparticles with energies $|\varepsilon| \geq \Delta$. This dynamic stabilization of regions with $\Delta^* < \Delta$ corresponds to rf stabilization and rf induced superconductivity in those regions [10]. It should be mentioned that this rf stabilization has been observed also in the transition of NbO_x layers to the normal conducting state [3b].

Nonlinearities in R (T,B) for Homogeneous Nb

Intrinsic nonlinearities, like R-increases due to heating, can be cast in a power series [4a].

$$R(T,f,B) = R(T,f, \approx 10mT)$$

$$[1+ \gamma^* (B/0.2T)^2 + \eta (B/0.2T)^4 + \ldots\ldots] \qquad (3.1)$$

where as scaling field for Nb $B_c(0) \approx 0.2$ T is used substituting $B_c(T)$. For intrinsic BCS nonlinearities $\gamma^*_{BCS} < 0.1$ is estimated as upper limit, whereas heating yields larger $\gamma^*(T)$ values given in the one dimensional case by

$$\gamma^* (T_o) = \Delta T/\partial R(T)/\partial T/R(T_o) \approx$$

$$R_{BCS} (T_o) (0.2T/B_c(T_o))^2 \, 2\Delta/kT_o^2 \left[\sum \frac{d_i}{\kappa_i} + R_k(T)\right] \qquad (3.2)$$

Here d_{Nb} and κ_{Nb} are thickness and thermal resistance of Nb, for sputtered Nb/Cu the interface resistance has to be added and, at least, the Kapitza resistance $R_k(T)$ toward the He-bath has to overcome. The heat transfer by phonons is given by their scattering at quasiparticles and phonons which in RRR > 100 Nb is with $l_{ph}(T<4K,<4GHz) \approx 2.6$cm [4a] very scarce and, hence, yields for homogeneous Nb walls (≤ 5 nm) ballistic heat transfer from the rf interaction volume to e.g. the $Nb/Nb_2O_{5-y}/OH/H_2O$-He-interface. Grain boundaries may scatter phonons but always the Kapitza resistance has to be overcome, yielding $\gamma^*(T) \geq 0.2$ increasing at $T_\lambda = 2.17$ K to $\gamma^* > 10$ by film boiling, as shown in Fig. 3.

Residual rf Magnetic Losses R^H_{res} and R_{hys}

As discussed in [10a] the Nb_2O_{5-y}-interface with normal conducting states $n_L(z \geq 0.3$ nm) yields inelastic surface scattering and coherent momentum transfer to the lattice staying finite for $T \rightarrow 0$ with the ITE $\tau(z^*)$ of Eq. (1.1) which yield [4a,b]

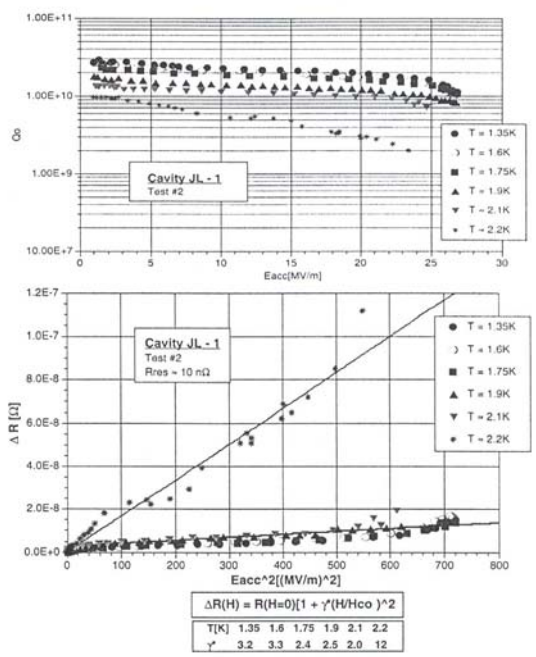

Fig. 3: R (T,B) results [12] show that for $R_{res} \approx 2.6$ nΩ $B_p \approx 180$mT > B_{c1} (1.6 K) = 160 mT is obtained with $\gamma^* = 0.25$ whereas after 2 years $R_{res} \approx$ 10nΩ yielded $B_p \approx 120$ mT at 1.6 K, where $R(T,H)\ B_{crit}(T)^2 \approx$ const holds. $\gamma^*(T)\ (B_p(T)/0.2\ T)^2$ shows a pronounced $\gamma^*(T)$ dependence [12b] with a jump at T_λ to $\gamma^* \geq 12$. The surface with $R_{res} = 2.6$ nΩ shows a slight $R^E \sim \exp(-c/E_p)$ degradation above $E^o \simeq 72$MV/m whereas $R_{res} =$ 10nΩ is accompanied by ITE and R^E (Eq. (1.3) above $E^o \simeq 45$ MV/m [12].

$$R_{res}(T,f) < 4 \cdot 10^{-9} \Omega (f/GHz)^2 \qquad (4.1)$$

The weak links filled with Nb_2O_{5-y} show the Josephson penetration depth $\sqrt{\lambda_J(T,H)} \approx \hbar/2e\mu_o\lambda_L(T)j_{cJ}(T)$. For weak links in a mean distance a_J with R_{bl} as leakage current resistance rf residual losses are obtained [10]

$$R^{WL}_{res}(T,f) \approx \frac{(2\mu_o\omega\lambda_L(T))^2}{1+(\omega\tau_J(T))^2} \frac{\lambda_J(T)^3}{a_J R_{bl}}$$
$$with\ 1/\tau_J = \frac{2e}{\hbar j_{cJ}(T) R_{bl}} \qquad (4.2)$$

as Josephson frequency. In weak links extending deep into Nb w >> λ_J, for $B_{rf} > B_{c1J} \simeq B_{c1}\ \lambda_L/\lambda_J$ Josephson fluxons penetrate causing hysteresis losses with the areal factor $2\lambda/a_J$ [11]

$$R_{hys}(T,\omega,B) \simeq 4\pi/3\mu_o\ \omega\ B/j_{cJ}\ 2\lambda/a_J \qquad (4.3)$$

For Nb $\lambda(T \leq T_c/2) \approx \lambda(0)$ and $j_{cJ}(T \leq T_c/2) \approx j_{cJ}(0)$ holds and, hence, below $T_c/2$ the rf residual losses show $R_{res}(T \leq T_c) =$ const and $R_{hys}\ (T \leq T_c/2) =$ const.

EXPERIMENTAL RESULTS

Experimentally, eigenfrequency changes $\Delta f/f_o$ and rf losses, e.g. the decay time $\tau = Q_o/\omega$ are the observables in

rf measurements, being related to the surface impedances by [10]:

$$\frac{\Delta\omega}{\omega_o} = \frac{i\oint dsZH^{\|2}}{2\omega_o\mu_o\int dVH^{\|2}} + \frac{\varepsilon_o/\mu_o\oint ds - Z^E E^{\perp 2}}{2i\omega_o\mu_o/\int dVH^{\|2}} =$$

$$i\frac{Z^H}{2G^H} + i\frac{Z^E}{2G^E}\ for\left\{H^{\|}, E^{\perp}\right\} << \left\{H_c, 10^8 V/m\right\}$$

For TEM modes $G^H = G^E$ holds, being weakened in TM-modes to $G^H \le G^E$ approaching $G^E \to \infty$ for TE-modes. In our analysis of the TM_{010}-mode we assume $G^H = G^E$ with $G^H \cong 290\ \Omega$ and peak field ratios $B_p/E_p = 2.5$ mT/MV/m and $E_p/E_{acc} \cong 1.8$

In [4a,b,9] the surface resistances R(T, ≈ 10 mT) ≈ $R_{BCS}(T) + R_{res}(T)$ have been quantified by the BCS theory, resulting in material parameters of Nb in 80 nm ($\gtrsim 2\lambda$) surface layers. At 1.5 GHz by annealing Nb at T ≈ 100°C R_{BCS} decreases by a factor 2 for RRR > 100 Nb and 1.5 for RRR ≈ 30 Nb to the identical lower level [4a], whereas the already degraded $\Delta/kT_c \simeq 1.85 < 2.05$ does not degrade further. Related to this R_{BCS}(10mT)- decrease is an increase of the R(B ≈ mT)-peak.

In Figs. 3 above $E_p \approx 10$ MV/m field dependencies are fitted by $\gamma^*(B/B_c)^2$. In the Nb cavity with the highest B_p obtained to date, γ^* (1.6 K) = 0.25, $R_{res} \simeq 2n\Omega$ and $B_p \approx 185$ mT > B_{c1} (1.6 K) ≃ 168 mT has been achieved [12a], degrading to $R_{res} \simeq 10n\Omega$ and $B_p \lesssim 120$mT by BCP after two years, where γ^* degrades to γ^* (T < T_λ) ≃ 3 jumping to $\gamma^* \simeq 12$ above T_λ shown in Fig. 3. γ* (T < T_λ) ≃ 2 and E_p -onsets at 40MV/m are standard as obvious in [4a, 7, 12b, 13] and Figs. 3 - 5. In Fig. 4 R(B)-dependencies and in Table 1 fit results are shown obtained in the TE_{011} and TM_{010}-modes of one cavity before and after UHV baking. The exponential R^E fits for TM modes to Eq. (1.3) are excellent being discussed in Sect. 5. Spun cavities show a very rough surface and, hence onset fields $E^*_p \approx 20$ MV/m in Fig. 5, which shifts to higher fields with BCP, whereas c increases. The c increases of Fig. 5 are fitted in [4a,13] by the expansion of $\delta R^E \propto E^{2n}$ starting with n ≥ 4 showing that this effect cannot be cast into a Taylor series. In Fig. 4b also such E^{2n} fits are shown with much larger errors than exp (-c/E)-fits in Fig. 4.

For the identification of this R^E component R(T,f,B) ≈ (R^H_{res}+$R^H_{BCS}(T_o,f)$ + R^E ($E^{\perp}$)) (1+γ* (B/0.2T)² +) of Eq. (3.2) has to be used, where the geometry factors are not correct for a non-linear interaction mechanisms i.e. local measurements are more appropriate. For Fig. 5 those are depicted as temperature maps in Fig. 6, showing no pronounced bad spot but critical $R^E(E^{\perp})$ – heating on a ring with $E \approx E_{crit}$ in this TM_{010}-mode, which change by surface smoothening to higher E_{crit} moving closer to the equator where R^E enhances $B^2R_{BCS}(T+\Delta T)$ via ΔT yielding breakdown on a ring with coarse spots. The smoothing of the rough, spinned surface by successive BCP [13] reaches $E_{crit} \approx 30$ MeV/m by successive higher onset field and higher n-values. Further E_{crit}-enhancements take advantage of EP yielding $E_{crit} \ge 40$ MeV/m for onset-fields $E^*_{rf} \approx 30$ MeV/m.

Whereas in Nb cavities using bulk Nb degradations with $\gamma^*(T < T_\lambda) \lesssim 3$ are typical – see, e.g., Figs. 3 – 6 or [4a, 12,13], sputtered Nb or heavily corroded Nb shows $\delta R \propto \omega B/j_{cJ}$ of Eq. (4.3) at T ≲ 2 K depicted in Fig. 7. As worked out in [11] those hysteresis losses are due to Jo-

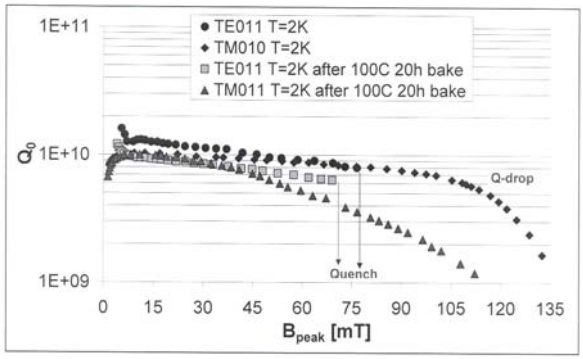

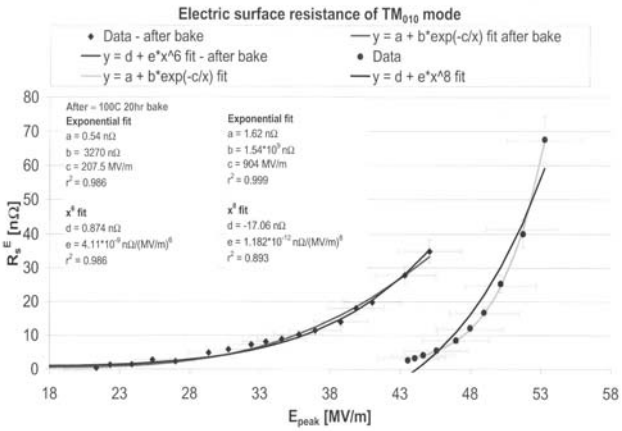

Fig. 4: a)Q_{versus} B_p in TM_{010} (= 1.47 GHz) and TE_{010} (= 2.83 GHz) modes without and with 100°C baking for 20 hr [14]. The Q (B ≃ 10mT) drop in the TE_{010} mode, like the low quench fields $B_p \simeq 10$mT are indicative for defects, which corrode faster as shown by the strong R_{res} increase by baking in Table 1.

Fig. 4b) Whereas the TE_{011} modes show no sign of $R^E \propto$ expc (-c/E_p) losses the TM_{010}-modes allow with Eq. (3.1) to deduce R^E (E) = $R(T_oB)/(1+\gamma^*(T_o)\ (B_p/0.2T))^2 - R(T_o \simeq 15mT)$ which fits to exp (-c/E) excellently, in lowest order (~ B^2) approximation [14].

Table 1: Fit constants to the data represented in Fig. 4 of modes in a multimode cavity containing defects causing low field Q(B) decrease and early breakdown in the TE-mode [14]. Also the strong degradation of R_{res} and γ^* by baking links to defects promoting corrosion.

	Before baking		*After baking*	
	TM_{010}	*TE_{011}*	*TM_{010}*	*TE_{011}*
γ @ 2.425 K	13	38	20	39
γ @ 2.2 K	15	34	26	62
γ @ 2 K	1.7	4.6	8.4	4.6
R_{res} [nΩ]	17	13	22	29

Josephson fluxon penetration along weak links. At higher fields and $R_{BCS}(T) \gtrsim R_{res}$ the $R_{hys} \propto \omega B/j_{cJ}$ – increase is negligible compared to the $\delta R \propto \gamma^*(B/B_c)^2$ increases shown in Fig. 8 with $\gamma^* \simeq 20 - 90$, as being discussed below.

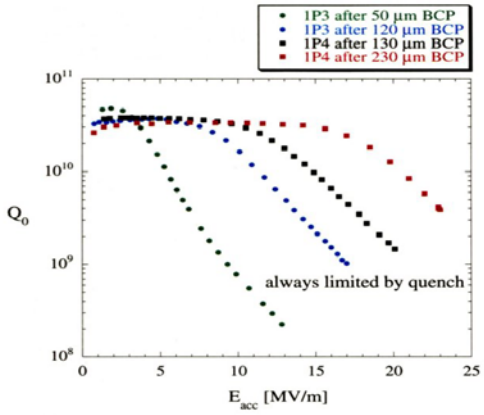

Fig. 5: R(2K,B) of a Nb TM_{010}-mode cavity at 1.3 GHz spun of RRR ≈ 30 sheath (P2 and P3). The onset fields E°_p = 6.3; 13.5; 19; 29 MV/m correspond to $\delta R^E \propto E^{\perp n}$ with n = 4; 6; 8; 10 after successive BCP smoothening up to 230 µm. Similar changes with BCP-smoothing are reported in [4a].

DISCUSSION

As mentioned in the introduction, [4a, 13] are not repeated in detail here, but new facts related to 100°C baking and prebreakdown and rf breakdown are elaborated. The BCS surface resistance R_{BCS} (T,f, ≈ $10B_{max}$) – see Sect. 2 – shows $\Delta/kT_c \simeq 1.85$, i.e. 10% below intrinsic values and reduced (surface) mean free paths l_s [4a] by oxidation sketched in Fig. 1. With 100°C baking (> 10h) R_{BCS} (T, ~1.5GHz, ≈ 10mT) is reduced to a saturatian value, e.g., by a factor 2 for high quality BCP cleaned Nb. By baking the R_{BCS}(T,f, B_{max}) peak grows [4a, 15]. All those baking observation are explained by the growth of NbO_x clusters in size yielding enhanced smearing of the BCS density of states (Eq. (2.2)) reducing R_{BCS}(< 10 GHz) and enhancing the R_{BCS}-peak, yielding for B ≥ B_{max} rf induced superconductivity [10], stabilizing those NbO_x-regions up to T_c and B_c of the bulk [3b].

Rf residual losses $R_{res}(T,f) \gtrsim 2n\Omega\ (f/GHz)^2$ are due momentum transfer by surface scattering being enhanced by localized states n_L in Nb_2O_5 and by the leakage current via those normal conducting n_L-states (Eq. (4.2)). Hence R_{res} grows by oxidation – see Table 1 or Fig. 4 and [4,13] – the more, the more defects exist in Nb acting as nucleation for crack corrosion. For extended weak links w>> λ_J (Eq. (4.2)) Josephson fluxon are created for fields above B_{c1J} causing hysteresis losses $R_{hys} \propto \omega B/j_c$ of Eq. (4.3). Those are observed not only for sputtered Nb films in Fig. 7 but for heavily oxidized Nb also [16]. Aside of the magnetic residual losses $R^B_{res} \propto f^{\alpha}$ ($\alpha \approx 1$-2) also standard dielectric losses of Nb_2O_5 or by interface tunnel exchange of conduction electrons n_m with localized states are found – see Eqs. (1.1) - (1.3). Those losses exists in TM-modes only and explain their higher rf residual losses, e.g. in Table 1. But with fields $E > E^{\circ}_{rf}$ of Eq. (4.3) exponentially increasing losses with $c = 2\kappa\Delta\varepsilon_r/e\beta^*$ occur, where the local electric field of Fig. 6 has to be used initiating via B^2R_{BCS} (T+ΔT) and B > $0.7B_p$ the rf breakdown. Shown in Fig. 4b is excellent agreement with theory in contrast to E^{2n} (n ≥ 4) fits. The increase of onset fields E° in Fig. 5 are related to smoothing of the surface decreasing ß* shifting the R^B_{BCS}-breakdown to the equator, as will be analyzed below.

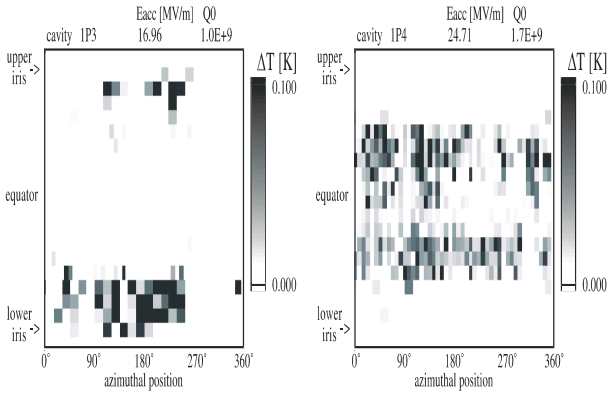

Fig. 6: Heat maps at different field levels for spun Nb cavities P3 and P4 of reactor grade Nb (RRR ≈ 30) at field just below the quench at B_{crit} showing in this field region an $E^{\perp}$-Q_o-drop with 6 ≤ n ≤ 12 in Fig 5 [4a]. The maximum temperature rise was 0.4 K in order to display also areas with lower heating. The rotational symmetric heatings, which do not show a pronounced spot typical for impurities or stripes for field emission, shifts with increasing E°_{rf} away from E_{max} towards B_{max} adding there to the temperature dependent losses $R^H(T)\ B^2$. For example for the $E_{acc} \simeq$ 17MV/m breakdown the heat pulse develops at $E_p \simeq$ 33MV/m and B ≃ 50mT and for $E_{acc} \simeq$ 25MV/m at $E_p \approx$ 40 MV/m but $B_p \simeq$ 100 mT.

The field dependences in Figs. 3 – 8 always contain for B ≳ 10 mT an $\gamma^*(T)\ (B/0.2T)^2$-increase. Remarkable is the jump of $\gamma^*(T_\lambda)$ in Figs. 3 and Table 1 by factors around 4 [4a, 13] proving the dominance of the Kapitza boundary resistance R_K over the thermal conductivity through Nb and proving that the BCS like B^2 increase is heating. The dominance of R_K is in line with ballistic heat transfer through 2 – 3 mm bulk Nb due the long phonon (26mm) and inelastic electron (~ 2mm) mean free paths [13] mentioned in Sect. 3.2. The $\gamma^*(T_\lambda)$ jump indicate also that Nb grain boundaries are not effectively scattering phonons for T ≈ T_λ.

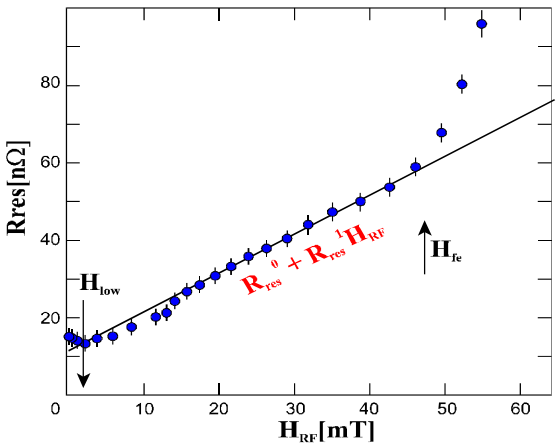

Fig. 7: Dependence of the residual resistance R (T ≤ 2K, B) on B_{rf} for a typical film on oxidized Cu with $a_J \simeq$ 0.1 µm. The solid line represents the linear fit used to define R_{res}^{o} and $R_{res}^{1} \propto R_{hys} \propto \omega B/j_{cJ}$ – see Eq. (4.3) and [16]

The other remarkable results shown in Fig. 3 and [12] are: a factor 4 higher R_{res} values relate to a factor 10 larger

$\gamma^*(T < T_\lambda)$ values and in Fig. 8 [16,17] for Nb films sputtered onto Cu γ^* is enhanced to values of about 60 decreasing to about 20 at 4.2 K. Whereas $\gamma^*(T < 2K) \simeq 0.25$ [12a] is in line with measured Kapitza resistances [14], $\gamma^* \simeq 2 - 90$ can neither be explained by any boundary resistance Nb/He or Nb/Cu measured to date. But the enhanced R_{res} accompanied by a γ^* increase by a factor 10 or the locally enhanced losses R_{hys} by weak links in Fig. 7 accompanied by $\gamma^* \simeq 90 - 16$ offer a plausible explanation by locally confined rf losses being transfered with negligible diffusive smearing to the Nb/He or Nb/Cu interface. Hence γ^* in Eq. (3.2) has to be multiplied by the energy pile-up, e.g., for Fig. 7 with hysteresis losses R_{hys} and R_{res} confined in weak links of $d(Nb_2O_5) \approx 2nm$ width in distances $a_J \approx 0.2\mu m$ enhances $R_{Nb/Cu}$ by a pile-up factor $r_k \simeq 2nm/a_J \approx 100$ confirmed by $\gamma^* \simeq 16 - 60$ in Fig. 8. The temperature dependence of $\gamma^*(T)$ [16] is in line with $R_{Nb/Cu} \propto T^{-4}$ in Eq. (3.2) and the fact that in Fig. 8 no $\gamma^*(T_\lambda)$ jump occurs, confirming our model of dominant interface resistances R_K adjacent to the origin of rf losses and that the interface Nb/Cu and Cu yields a diffusive heat transfer with r_k diminuishing to $r_k \simeq 1$ at the Cu/He interface.

In the case of typical, natural oxidation with some weak links depicted in Fig. 1 yielding $\gamma^*(T < T_\lambda) \approx 2$ a pile-up factor $r_K \simeq 1nm/a_J \approx 10$ is line with the factor 10 enhancement of $\gamma^*(T < T_\lambda)$ as compared to $\gamma^*(< T_\lambda) \simeq 0.25$ [12]. This concept of energy pile-up r_K transferred ballisticly to thermal interfaces resistances is obvious also in Tabel 1, where the TE-mode limitation by a defect shows $\gamma^*(T < T_\lambda)$ being a factor 3 larger than in the TM mode of the same cavity. Also the fact that $\gamma^*(T<T_\lambda)$ is enhanced by those defects as compared to TM modes prove the validity of the energy pile-up factor r_k. In [14] the $\gamma^*(T_\lambda)$ jump is explained semiquantitatively.

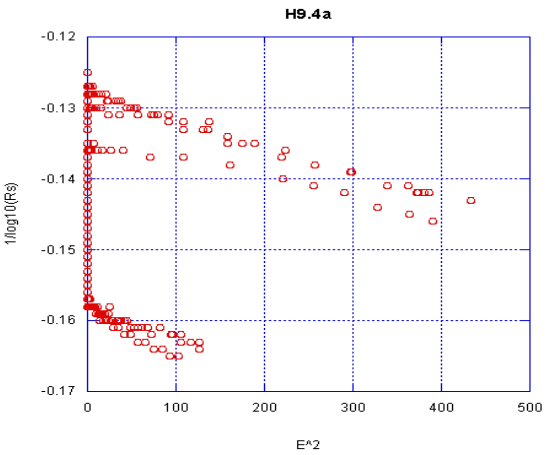

Fig. 8: Plot of 1/log R (T,E) versus E^2 of a 3μm Nb film on Cu. The straight lines for $R(T,E) > R_{res} + R_{hys}$ prove $1/\ln R\,(T + \Delta T,B) \propto (T+\Delta T)/\Delta$ with $\Delta T \propto E^2$. Oxidized Cu with $a_J \lesssim 0.1\mu m$ shows an E^2 decrease with $\gamma^*(2K) \simeq 55$ decaying to $\gamma^*(4.2K) \simeq 20$ [16,17].

The breakdown in Figs. 3 -8 is due to thermal runaway via $R_{BCS}(T)$ needing higher orders in ΔT than γ^* alone in Eq. (3.1). But $\gamma^*(< T_\lambda) > 0.2$ acts as signature for defects, as shown in Fig. 4, by the defect induced breakdown in the TE-mode. In the TM-modes in Fig. 3 – 5 the $\exp(-c/E_p)$ triggers the rf breakdown. As shown in the heat maps in Fig. 6 belonging to Fig. 5 the $\exp(-c/E)$ increases causes heating amplifying $R_{BCS}(T)$ triggering rf breakdown. This amplification needs higher order, as in Fig. 8 for $\gamma^* > 10$. The combined action of $\exp(-c/E)$ amplifying $R_{BCS}(T + \Delta T,B)$ is obvious in Fig. 6 showing rf breakdown at $E \approx E_p/3 > 40$ MV/m, $B \approx B_p > 70$ mT and $E_{acc} \simeq 25$ MV/m. The crucial influence of enhanced γ^* by $r_k > 10$ is obvious in Fig. 4 by the B_{crit} being reduced by 20% by $\gamma^* \approx 8$ after baking or in sputter cavities by the low $E_{acc} \lesssim 15 - 25$ MeV/m decreasing with γ^* increases [16].

REFERENCES

[1] a) P. Kneisel, Proc. 1, Workshop an rf superconductivity (KfK 3019,1980), p. 27
b) P. Kneisel et al., Proc. 6. Workshop on rf superconductivity (CEBAF, 1993), p. 628

[2] P. Kneisel, Proc. 7. Workshop on rf superconductivity (IN2P3, 1996), p. 449 and this conference

[3] a) A. Das Gupta et al, J. Appl. Phys. 47, 2146 (1976)
b) W. Schwarz and J. Halbritter, J. Appl. Phys. 48, 4618 (1977)

[4] a) J. Halbritter, Proc. 10 Workshop on rf superconductivity, 2001, Tsukuba, p. 292
b) J. Halbritter, J. Less-Common Met. 139, 133 (1988) and Appl. Phys. A.43, 1 (1987)
c) J. Halbritter, Surf. Sci. 159, 509 (1985) and J. Appl. Phys. 58, 1320 (1985)

[5] a) M. Grundner and J. Halbritter, J. Appl. Phys. 51, 397 and 5396 (1980)
b) J. Halbritter, IEEE Trans EI-20, 671 (1985) and Appl. Phys. A39, 49 (1986)

[6] M.E. Cuneo et al., IEEE Trans. Dielectr. and Elect. Insul. 6, 469 (1999)

[7] a) J. Halbritter, Z. Phys. B31, 19 (1978)
b) J. Halbritter, IEEE Trans Appl. Supercond. 11, 1864 (2001)

[8] P. Kneisel et al., Proc. 6. Workshop on rf superconductivity (CEBAF, 1993), p. 617

[9] J. Halbritter, Z. Phys. 266, 209 (1974) and J. Supercond. 4, 341 (1991)

[10] J. Halbritter, Report 08.02.02 P06B (IKP, FZK, 1979)

[11] J. Halbritter, J. Superconductivity, 8, 691 (1995)

[12] a) P. Kneisel, Proc. 7. Workshop on rf superconductivity, 1995, cif sur Yvette (IN2P3, 1996), p. 449
b) P. Kneisel et al., Proc. 8 Workshop on rf superconductivity, Oct. 1997, Abano Terme (V. Palmieri, A. Lombardi Eds, LNL-INFN-Rep. 133, 1998), p. 463

[13] J. Halbritter in Superconductiving Materials for high Energy Colliders (Eds. L. Cifarrelli and L. Moritata, World Scienfic, 1999), p. 59

[14] G. Ciovati et al., this conference and private communication

[15] P. Kneisel, this conference and private communication

[16] J. Halbritter, submitted to J. Appl. Phys.

[17] S. Calatroni, this conference